RAA 2021 Vol. **21** No. **7**, 181(8pp) doi: 10.1088/1674-4527/21/7/181

http://www.raa-journal.org *http://iopscience.iop.org/raa*

Research in Astronomy and Astrophysics

A low-cost and high-performance technique for adaptive optics static wavefront correction

De-Qing Ren[1], Tian-Yu Zhang[2,3,4] and Gang Wang[2,3]

[1] California State University Northridge, Department of Physics and Astronomy, Northridge, CA 91330, USA
[2] National Astronomical Observatories/Nanjing Institute of Astronomical Optics and Technology, Chinese Academy of Sciences, Nanjing 210042, China; *tyzhang2019@niaot.ac.cn*
[3] CAS Key Laboratory of Astronomical Optics and Technology, Nanjing Institute of Astronomical Optics and Technology, Nanjing 210042, China
[4] University of Chinese Academy of Sciences, Beijing 100049, China

Received 2020 September 8; accepted 2021 March 12

Abstract Non-Common Path Error (NCPE) is one of the factors that limit an Adaptive Optics (AO) system from delivering ultra-high performance. To correct the NCPE associated static aberration, we propose a simple but robust and high-performance pupil-plane based wavefront measurement and correction technique, which can copy a single-mode fiber generated perfect wavefront to the AO system via an iteration optimization process, and the NCPE can be effectively corrected by directly commanding the Deformable Mirror (DM) of the AO system. Compared with the previous focal-plane based approach that uses focal plane based Point Spread Function (PSF) for correction evaluation, the pupil-plane based approach can be reliably and rapidly converged to a global optimization result and provides better performance, in particular for an AO system with a large initial static wavefront error. This technique we proposed can be implemented in astronomical AO systems where extremely high performance is required.

Key words: astronomical instrumentation: adaptive optics — astronomical instrumentation: high angular resolution — astronomical techniques: high angular resolution

1 INTRODUCTION

To correct atmospheric turbulence perturbation induced wavefront errors and to achieve diffraction-limited imaging performance, Adaptive Optics (AO) systems are being employed for ground-based observations. Recently, extreme adaptive optics (ExAO) was proposed for high-contrast exoplanet imaging. ExAO systems were optimized for extremely high performance, which will be able to deliver a Strehl ratio (SR) better than 0.9 and a contrast up to 10^{-7} for coronagraphic imaging within a few λ/D to the host star. For such a challenging task, studies show that one of the performance limitations is the Non-Common Path Error (NCPE) that is introduced by the physical separation between the AO wavefront sensor (WFS) path and the science camera path (Ellerbroek et al. 2010), which cannot be measured by the AO WFS and thus cannot be corrected by the AO closed loop system. Therefore, this static optical error must be effectively removed before the ExAO can be utilized for high-contrast exoplanet imaging.

The previous approaches adopted by ExAO for the NCPE correction are complicated and time-consuming, since a dedicated hardware system will be needed to achieve ultra-high performance. They adopted a two-step approach that involves two independent procedures for the measurement and correction, respectively. In the first step, only the wavefront error is measured, such as using the phase diversity (PD) algorithm (Gonsalves 1982) or a dedicated interferometer (Wallace et al. 2011; Campbell et al. 1999), in which no wavefront error correction is applied and the measured results are output as Zernike polynomial. For example, the traditional PD algorithm examines a couple of focused and defocused images to measure wavefront errors only (Hartung et al. 2003; Sauvage et al. 2007). In the second step, the measured wavefront error of the Zernike polynomial is imported to an AO system. Since the first step in the measurement relies on traditional general wavefront measurement techniques such as the PD and interferometer that only provide the wavefront measurement expressed by the Zernike polynomial, one needs to consider how to input this result into an existing AO system to correct this wavefront error. In principle, in the second step of the wavefront correction, one can manually input the measured Zernike polynomial to an existing AO system and then command its Deformable Mirror (DM) to correct this error measured in the first step. Of course, one can also modify an existing AO code to accommodate the Zernike polynomial generated in the first step. Nevertheless, there are still some potential issues for this two-step measurement-correction approach. The measurement accuracy of the PD technique is limited by the number of Zernike polynomial orders included. For example, the PD for the Very Large Telescope (VLT) only measured 15 orders of Zernike polynomials (Hartung et al. 2003), and the high frequency wavefront message is missed because of the use of the polynomial. The order of the measured Zernike polynomial may not exactly match what the DM can correct. In addition, because of separation of the wavefront measurement and the AO correction, the alignment of the measured wavefront with the AO system such as the wavefront orientation is also an issue, which further limits the final performance that the AO can deliver. Although the dedicated interferometers can produce high accuracy wavefront measurements (Wallace et al. 2010, 2011; Hinkley et al. 2011), an interferometer is sensitive to the vibration, stray light and temperature change in the measurement environment, which may degrade its actual performance. Because of the inherent nature of the two-step approach, the errors introduced in the measurement process will be eventually added into the correction process (Sauvage et al. 2007; Hartung et al. 2003; Wallace et al. 2011), which limits the final correction performance.

In our previous work, based on a multi-core personal computer and LabVIEW software programming, we developed a portable AO system (Ren et al. 2010; Ren & Dong 2012). This portable system incorporates off-the-shelf commercial components, and is further developed for high-contrast exoplanet imaging with 4-meter class telescopes, including the ARC 3.5-meter telescope located at Apache Point Observatory, USA and the 3.58-meter Telescopio Nazionale Galileo (TNG) located at Roque de los Muchachos Observatory on the island of La Palma, Spain. As a visiting instrument, the NCPE must be corrected rapidly in an efficient way before any AO observation can be conducted on the same day. As such, we proposed a focal-plane based wavefront sensing and correction approach, in which both the wavefront error measurement and correction are integrated in a single step and optimized in our SPDG algorithm until good performance is achieved. Since it relies on the AO system's DM to directly correct the wavefront and avoids use of the intermedium wave reconstructed by the Zernike polynomial, the correction fully matches the DM correction capability (Ren et al. 2012). This approach utilizes the focal plane science camera to evaluate the Point Spread Function (PSF) image, and directly commands the DM to correct the wavefront error. However, since the measurement is done with the PSF on the focal plane where the PSF intensity in the area outside the Airy disk is weak and is rapidly dominated by the WFS camera's readout noise as well as the camera's limited dynamic range, the focal-plane based approach needs a large amount of time to optimize and achieve acceptable performance, and in the worst case it may deliver a local optimization result, instead of a global one, which further limits this approach's performance.

In this article, we propose a novel pupil-plane based measurement and correction technique to measure and correct the NCPE simultaneously in a single step. By implementing an iteration optimization algorithm such as the stochastic parallel gradient descent (SPGD) approach, a perfect reference wavefront, which is free of optical aberration, is used to provide an effective guide for optimization in the correction process, and thus it can significantly speed the correction process and achieve a global optimization for the NCPE correction. Since the measurement is done on the pupil plane, the previous weaknesses associated with the PSF measurement on the focal image plane are avoided. The hardware setup is relatively simple, and this approach is robust and can deliver excellent performance at different circumstances with different initial wavefront errors. This article is organized as follows. In Section 2, we will describe the general principle of our pupil-plane based approach dedicated to the AO NCPE correction. In Sections 3 and 4, we present our laboratory experimental test and result respectively, in which we describe our pupil-plane based wavefront optimization result. In Section 5, we compare different approaches for the NCPE correction. Finally, we discuss our conclusion in Section 6.

2 WORKING PRINCIPLE

Figure 1 illustrates the schematic diagram of the AO system we used for the NCPE correction. The light from a single-mode fiber (SF1) is collimated by lens L1 and reflected by a tip-tilt mirror (TTM) and a DM, which can be commanded to correct possible NCPE aberration. A non-polarized beam-splitter (BS) directs part of the incoming light to the AO WFS path and science image path. The AO WFS path consists of lenses L2 and L3, a microlens array (MLA), and a high-speed camera (C1) for real-time AO wavefront sensing. At the science image

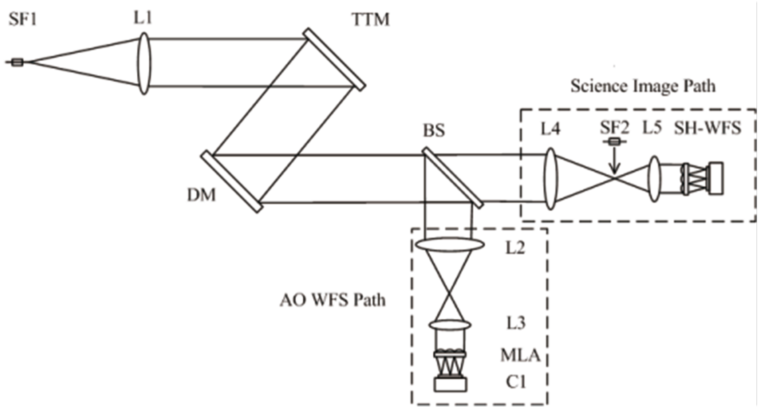

Fig. 1 The schematic diagram of the AO NCPE measurement and correction system.

Table 1 Hardware Required for the Construction of the Pupil-based SPGD Measurement-correction System

Method	Hardware
SPGD pupil-plane method	Single-mode-fiber assembly (SF2), collimator lens, SH-WFS, C-mount camera.

path, the science camera (not shown), which is located on the AO output focal plane immediately after the science image lens L4, is replaced by an assembly that consists of a lens L5 and a Shack-Hartman wavefront sensor (SH-WFS) during the period of the NCPE measurement and correction. Please note that the SH-WFS is used for the NCPE measurement and correction only, and it is not a part of the AO closed-loop system for AO real-time wavefront correction, for which the AO has its own WFS displayed in the AO WFS path in this figure. The L5 generates an exit pupil image on the surface of the MLA in the SH-WFS, where the measured wavefront is sampled and imaged. A second signal-mode fiber (SF2), which only allows the fundamental wavefront mode to pass through and thus is free of optical aberration, can be inserted into the focal point of the lens L5 to generate a perfect reference wavefront for the NCPE wavefront measurement and correction. Each time, either the reference light (SF2) or the AO light source (SF1) will be located in the optical path to be imaged by the system. After NCPE wavefront measurement and correction are completed, the SF2, L5 and the SH-WFS assembly in the AO image path will be removed from the optical path, and the science camera can be switched back to the optical path for regular AO closed-loop imaging.

Table 1 lists the extra hardware required to construct our pupil-based SPGD measurement-correction system. The single-mode-fiber assembly, including both an HeNe cylindric laser light source, a single-mode fiber patch (SF2) and the associated mount, was purchased from Thorlabs, Inc. The output end of the single-mode fiber and its mount are installed on a standard pedestal-style post holder (purchased from Thorlab, Inc), which allows manual alignment in the XYZ directions. The collimator lens is a standard mounted lens (purchased from Thorlab, Inc), and it has a focal length of 50 mm. In our actual field observations, we rely on an MLA (purchased from Thorlab, Inc) and a standard C-mount video camera to reconstruct the SH-WFS assembly. The MLA is glued on a small aluminum tube that is directly screwed into the C-mount camera. The extra total physical size required for the NCPE correction is 150 mm immediately after the AO science image focus, which is used to accommodate the collimator lens and the small SH-WFS assembly. Since all components are commercially available, the cost of the NCPE correction system is not expensive. When implementing the NCPE correction, the AO science camera is moved out of the optical path to provide the necessary physical space, and it is repositioned back after such a correction is completed. Since a large amount of off-the-self components are utilized, the cost required for the hardware for the NCPE system is quite low. Please note that in this experiment, we used a standard SH-WFS assembly previously purchased from Thorlab, Inc, which includes its software for the characterization of the corrected wavefront error by measuring the Zernike polynomials, and such a characterization is not necessary for our actual field observations.

The following alignment procedure is involved to take data that will be utilized for the measurement and correction of the NCPE. First, the AO SF1 image is recorded by the SH-WFS camera in the science image path, which includes all of the static wavefront information, as depicted in Figure 2(a). This standard SH-WFS focal plane image consists of an array of spots, in which each microlens sub-aperture forms a PSF spot of the

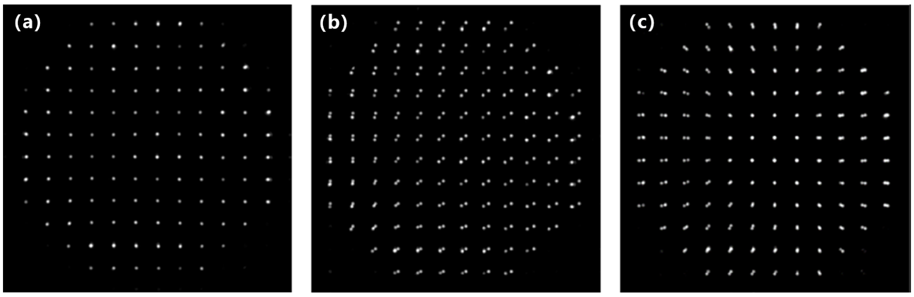

Fig. 2 (a) Recorded SH-WFS image on the AO science image path. (b) The original image taken before the alignment of the two fiber images. (c) The final image taken after a good alignment of the two fiber images.

image. Thus, any deviation from the perfect spot position will be an indication of associated wavefront aberrations that need to be corrected.

Secondly, the AO SF1 light source is blocked and the single-mode fiber SF2 is inserted into the SH-WFS focus to replace the AO SF1 light source. The image of the SF2 serves as the perfect wavefront and thus its spot array is used to define the perfect spot position in each sub-aperture that has no wavefront error. During this process, the previously recorded AO SF1 spot array is displayed as a background image in an output display window, as shown in Figure 2(b). The SF2 is installed on an XYZ translation stage, and is moved as close as possible to overlap with the spot array previously generated by the SF1. An overall image shift between SF1 and SF2 corresponds to a tip-tilt error between these two wavefronts, and thus a small shift will be preferred to reduce the correction burden applied to the DM. Figure 2(b) features the initial image before these two fiber images are aligned, and Figure 2(c) shows the final image after the two fiber images are well aligned, by carefully moving the SF2 single-mode fiber via the XYZ translation stage. Now, since the AO system has some NCPE, the spots between these two images generated by these two fibers cannot be exactly overlapped, as depicted in Figure 2(c), which must be corrected by the AO DM until all spots are exactly overlapped. Please note that in principle the quality of lens L5 in Figure 1 will not affect the correction results of the NCPE, since both the AO image and the SF2 reference optical paths go through the same portion of this lens, and any potential wavefront error induced by the lens L5 will be removed by the subtraction of the spot centroid in each sub-aperture between these two beams, in our NCPE measurement and correction.

Once the above alignment is done, we can command the AO DM to change the DM's shape to correct the NCPE, until all spots generated by SF1 and SF2 are exactly overlapped. To achieve this goal, we can implement an iterative optimization approach. For our NCPE correction, we use the well-known SPGD algorithm (Vorontsov et al. 1997; Vorontsov & Sivokon 1998; Vorontsov & Yu 2004). It applies small random perturbations to all control parameters (i.e., the voltages of DM actuators) simultaneously and then evaluates the gradient variation of a metric function J. The control signals are updated in an iterative process using the following rule,

$$u^{k+1} = u^k - \gamma \delta J^k \delta u^k \,, \tag{1}$$

where k is the iteration number; $u = u_1, u_2, ..., u_n$ is the voltages of DM actuators, n is the number of effective actuators; γ is a constant gain coefficient which is positive for minimizing and negative for maximizing the metric function J; It is in the range $0 < \gamma < 0.01$, and in our test a value of 0.002 was used. δu denotes small random perturbations such that all elements of the δu have identical amplitudes but pseudorandom signs (according to a Bernoulli distribution). An initial 0 value for all elements of δu was applied in our test. δJ is the variation of the system's performance metric function,

$$\begin{aligned} \delta J &= J(u + \delta u) - J(u) \\ &= J(u_1 + \delta u_1, ..., u_n + \delta u_n) - J(u_1, ..., u_n). \end{aligned} \tag{2}$$

To improve the estimation accuracy of δJ, a two-sided perturbation is defined as follows,

$$\delta J = J_+ - J_- = J(u + \delta u/2) - J(u - \delta u/2). \tag{3}$$

Even though a constant gain coefficient γ was used for our test, a variable constant can also be used to accelerate the convergence,

$$\gamma^{k+1} = \gamma^k J^k. \tag{4}$$

Considering the correction system with the goal to remove the NCPE and achieve a perfect plane wavefront on the exit pupil of the AO system image path, the SF2 generated wavefront is regarded as a perfect wavefront to provide an explicit guide for the optimization direction at each iteration in the correction process. The metric function J is used to evaluate the wavefront difference between the perfect reference and actual AO waves. For the SH-WFS with m effective sub-apertures, we define the metric function J to be optimized as

$$J = \sum_{i=1}^{m} (x_i - x_i')^2 + (y_i - y_i')^2 \,, \tag{5}$$

where $(x_i,\, y_i)$ and $(x_i',\, y_i')$ are the centroid coordinates of AO (generated by SF1) and the reference (generated by SF2) light sources in each microlens sub-aperture i of the SH-WFS, respectively. As the above equation indicates, the metric function J will have a minimum value after the optimization, which corresponds to a wavefront difference minimum between the reference and AO paths. In the perfect case, $(x_i,\, y_i)$ and $(x_i',\, y_i')$ are overlapped at every microlens of the WFS, so that we have $(x_i,\, y_i)$ = $(x_i',\, y_i')$ and thus J is equal to 0 and a minimum is achieved. In a real operation, because of the measurement noise, the J cannot be optimized to be 0, and a small value will be an indication of good performance for the optimization. Please note that SPGD Equations (1) to (4) were used previously by other researchers for the closed loop operation of an AO system in which no WFS was needed (Vorontsov et al. 1997; Vorontsov & Sivokon 1998; Vorontsov & Yu 2004). For our metric function Equation (5), as we will see in our laboratory test in the next section, it will deliver an excellent PSF correction with an SR of 0.995, and both the $(x_i,\, y_i)$ and $(x_i',\, y_i')$ are overlapped at every microlens after our SPGD optimization (see Fig. 6), which indicates a global optimization is achieved. Please note that the metric function is not only a simple overlap between two independent light sources. It incorporates an SH-WFS to record the image position of all the effective sub-apertures, i.e., the wavefront phase information. Then, the recorded perfect reference wavefront is copied to the AO system by the SPGD algorithm. Therefore, after the correction, the NCPE is effectively corrected.

Once the above SPGD correction is done, the DM voltages are locked and are used as the DM reference voltages for the AO system. The DM reference voltages correspond to a perfect wavefront that the AO will correct for. Therefore, by simply replacing the DM reference voltages in our AO system, the single-mode fiber SF2 generated reference wavefront is copied to our AO system for real-time closed-loop operation. Also, by directly commanding the DM in the wavefront measurement and correction in each of our SPGD optimization iterations without the need for intermedium wavefront reconstruction, we are able to integrate both the wavefront measurement and correction in a single step.

3 LABORATORY TEST

Figure 3 displays the experimental setup in the laboratory. An HeNe laser light source of λ=632.8 nm wavelength is used for this test via the single-mode fiber SF1. According to the waveguide theory a single-mode fiber only allows the fundamental wave mode to pass through and thus can provide a perfect wavefront. The TTM is a fast-tilting platform provided by PI Corporation. The DM was purchased from the ALPAO Corporation with 97 actuators (in an 11 $\times$ 11 configuration, excluding those actuators in the four corners). The SH-WFS was purchased from Thorlabs, Inc (WFS150-5C). Thorlabs SH-WFS provides a function of user reference pupil, which allows users to define a reference wavefront that has zero wavefront. Only 90% of the beam with a 3-mm diameter is used to measure the wavefront and PSF images. To measure and correct the NCPE, we wrote a dedicated LabVIEW code to grab images from the SH-WFS and command the DM with the SPGD algorithm discussed previously. Zernike polynomials are measured by relying on the software provided by Thorlabs, for the purpose of performance evaluation only, although this is not necessary for our NCPE measurement and correction.

The AO NCPE measurement and correction consist of these procedures for the system alignment and measurement-correction, respectively:

1. Recording the reference wavefront.

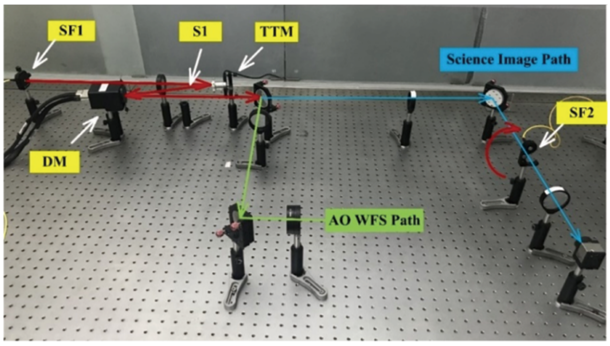

Fig. 3 The experimental setup of the AO system for the NCPE measurement and correction.

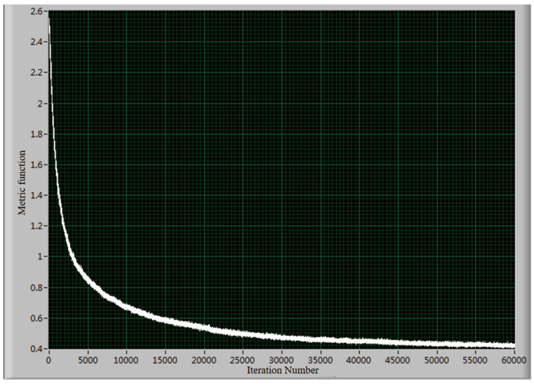

Fig. 4 Metric function evolution as a function of iteration number.

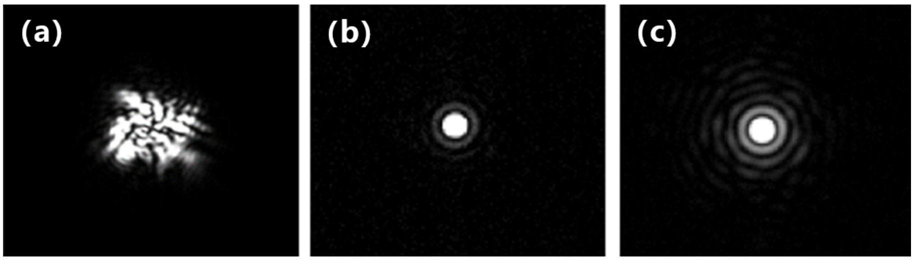

Fig. 5 (a) Initial focal plane PSF image. (b) and (c) are the PSFs with different exposures achieved after the NCPE correction.

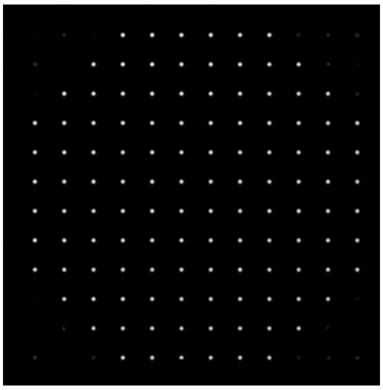

Fig. 6 The final spot image generated by the two fibers after the NCPE correction. Compared with Fig. 2(c) before this correction, the spots from both fibers are exactly overlapped.

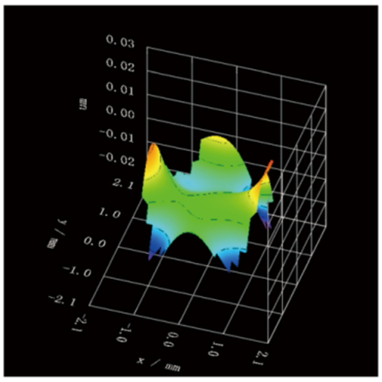

Fig. 7 The residual wavefront map after the NCPE correction.

Close shutter S1 and insert the SF2. This only allows the reference wavefront to be measured. The SH-WFS will record the reference wavefront's centroid coordinates of all effective microlenses. The corresponding centroid coordinates are recorded and serve as the reference wavefront. Since the quality of the reference wavefront directly affects the final correction result, we therefore rely on a single-mode fiber SF2 as the light source, which is free of optical aberration. Each reference centroid coordinate in each sub-aperture will provide a guide direction during the NCPE correction. Any AO wavefront error is measured relative to these centroid coordinates of this reference wavefront. Please note that the reference image can be recorded in advance before the correction.

2. NCPE correction.

Open the shutter S1 and remove the SF2 out of the optical path. This only allows the AO NCPE to be measured and corrected. A dedicated LabVIEW code was developed to control the DM according to the SPGD algorithm that optimizes all the DM actuators' voltages by evaluating the metric function J, according to Equation (1) and Equation (5). Figure 4 features our LabVIEW graphical user interface (GUI) in the SPGD optimization process for the evaluation of the metric function J as a function of the correction iteration number. When the metric function J has no significant reduction, the correction can be stopped and the DM voltages are automatically saved. Please note that the final metric function J and the residual wavefront error do not have a linear relationship. In fact, an iteration value of 40 000 in Figure 4 has almost no difference with a value of 60 000 in terms of the residual wavefront error or the final SR. With a commercial computer, the correction process takes about 45 minutes, which is a good value for a system with a large NCPE. The required SPGD optimization time is a function of the magnitude of the aberration to be corrected. For a smaller NCPE, 5 minutes will be enough to deliver a good correction result. Please note that here the AO system is optimized for high-contrast exoplanet imaging, where ultra-AO performance is required. For the case of a low SR such as an SR of 0.8 as required for other general applications (Burke et al. 2015), the required optimization can be significantly reduced. Once the best wavefront is achieved, the DM voltages are saved and applied to the AO system by replacing the existing AO DM reference voltages so that high SRs are achievable for the AO closed-loop operation. Please note that such an NCPE correction only needs to be done once for an AO system, if the system is installed in a stable platform.

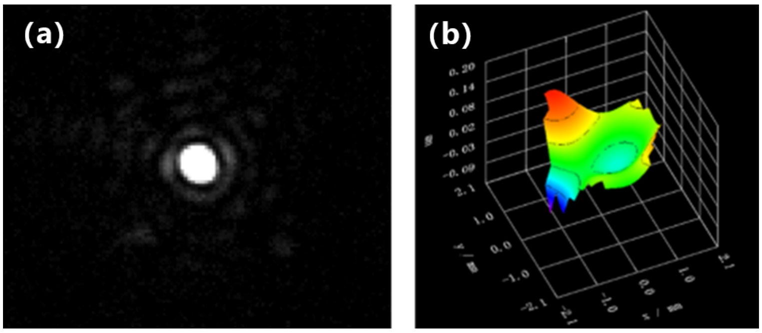

Fig. 8 (a) The PSF image after the SPGD focal plane correction. (b) The wavefront map after the SPGD focal plane correction.

4 EXPERIMENTAL RESULTS AND ANALYSIS

Figure 5(a) features the focal plane PSF image, before the NCPE correction. As shown, the initial focal plane PSF has a large initial wavefront error, with a peak-to-valley (PV) and a root mean square (RMS) of 766-nm and 110-nm, respectively, mostly contributed by the DM's residual wavefront error, since the ALPAO DM we used generally has a large initial wavefront error. After the NCPE correction, the wavefront error is dramatically reduced. Figure 5(b) and Figure 5(c) depict the AO focal plane PSF images with different exposure times, after the NCPE correction. Figure 5(b) features the PSF image with a proper exposure, while Figure 5(c) displays the PSF with a 10-time overexposure, which provides more details to see the diffraction pattern. As is apparent, the wavefront error is greatly reduced after the NCPE correction. The PV and RMS wavefront errors are reduced to 45-nm and 7-nm, respectively. The metric function decreases from the original value of 2.6 to 0.4 after the SPDG optimization by commanding the AO DM. Figure 6 shows the SH-WFS spot image generated by both the AO image and the reference fiber optical paths after the SPGD optimization and NCPE correction. Now, compared with Figure 2(c) before the correction, the spots generated by these two fibers after the correction are exactly overlapped, which indicates that the reference wavefront is effectively copied to the AO system.

Table 2 lists the associated Zernike coefficients of the wavefront error, before and after the NCPE correction. After the correction, all the Zernike coefficients are reduced, which indicates that the NCPE in the AO system is effectively corrected. The corrected wavefront map is displayed in Figure 7. The SR can be estimated by applying the following rule

$$SR = e^{-\sigma^2}, \tag{6}$$

where σ is the RMS wavefront error in radian. The 7-nm RMS error corresponds to 0.07 in radian at the 632.8-nm wavelength. This yields an SR of 0.995. As shown, the SR is improved from the initial 0.300 to 0.995, which clearly demonstrates that our pupil-plane based NCPE measurement and correction approach can deliver excellent performance.

Table 2 AO System Wavefront Error Expressed by the Zernike Polynomial Coefficients

Zernike coefficient	Initial error	Corrected error
Astigmatism y	–0.020	0.002
Astigmatism x	0.091	0.003
Trefoil y	–0.006	0.001
Coma x	0.007	–0.002
Coma y	0.025	–0.001
Trefoil x	–0.012	0.001
Tetrafoil y	0.006	0.000
Secondary Astigmatism y	–0.005	0.001
Primary Spherical	–0.023	0.001
Secondary Astigmatism x	0.005	0.000
Tetrafoil x	–0.056	0.005

5 THE COMPARISON EXPERIMENT

In this paper, we introduced in detail a new pupil-plane approach for the NCPE measurement and correction. To fully evaluate the advantage of our pupil-plane approach, we will compare it with our previous focal-plane approach under the same experimental condition. The configuration of the focal-plane correction system is a typical AO system, except that on the AO focal plane, the science camera is utilized for the evaluation by using the focal plane PSF, by implementing the SPDG optimization algorithm. Details on the focal plane correction approach are discussed by our previous publication (Ren et al. 2012). When an AO system has a large static wavefront error, it is difficult to be effectively corrected by the focal plane approach. For the above AO static wavefront error, an acceptable result is obtained by manually modifying the SPDG optimized parameters several times during the optimization process, with the correction result shown in Figure 8. Now, the RMS error is 50-nm, which corresponds to an SR of 0.782. The focal-plane based correction takes about 150 min, which is much longer than that of the pupil-plane based approach.

The performances of both focal-plane and pupil-plane correction approaches are conducted and compared under the same experimental condition. In summary, when large initial static aberrations are present in an AO system, the focal plane correction approach is more difficult to conduct to deliver good performance and it is easier to drop into a local optimization, which limits its performance. The experimental results affirm that the pupil-plane correction approach we presented in this publication can deliver much better performance, with much less required time for the optimization. Compared with the focal-plane method, the SR of pupil-plane method improves by 27% and the correction speed outperforms by a factor of 2.3. More importantly, it is easy to converge to a global optimization result, due to a perfect reference wavefront being used to guide the optimization direction. Sauvage et al. (2005) relied on a dedicated PD system for the AO NCPE correction. The experimental result indicates that the corrected SR is 0.93 at a wavelength of 632.8-nm (Sauvage et al. 2005). Recently, the PD technique could yield an SR of 0.95 at the wavelength of 632.8-nm for an AO system correction (Wang et al. 2017). Here, the pupil-plane approach we proposed delivers a better SR up to 0.995.

6 CONCLUSIONS

In this publication, a technique for fast and effective AO NCPE measurement and correction is demonstrated. This technique is based on the pupil-plane wavefront evaluation approach and is realized by implementing the SPGD iteration optimization algorithm that directly commands the DM, until all the SH-WFS spots generated by the AO science image path and those that are generated by a perfect reference wavefront are exactly overlapped. That is, the perfect reference wavefront is effectively copied by the AO system to remove any potential NCPE. Since the reference wavefront is utilized to guide the optimization direction, global optimization results can be achieved fast and reliably, which ensures that better correction is achievable than the traditional focal-plane based evaluation approach. Compared with other complex measurement techniques, such as wavefront measurement that relies on dedicated interferometers, our pupil-based wavefront correction technique integrated both wavefront measurement and correction in a single step by directly commanding the AO DM via the SPDG optimization. With a perfect reference wavefront provided by a single-mode fiber, an SR of 0.995 is achieved from an original value of 0.300, at the 632.8-nm test wavelength.

Since our pupil-based SPGD correction is based on the numerical iteration optimization, any local and temporal disturbance such as a short-period vibration or local air turbulence will only disturb a few iterations, which can be compensated by other following iterations and thus will not degrade the final optimization performance. It is a robust technique, which makes it more practical to be implemented in different environmental circumstances. This work provides a novel and robust technique for effective AO NCPE corrections.

References

Burke, D., Patton, B., Huang, F., Bewersdorf, J., & Booth, M. J. 2015, Optica, 2, 177

Campbell, E. W., Bauman, B. J., Dillon, D. R., & Olivier, S. S. 1999, High-accuracy Calibration of an Adaptive Optics System Using a Phase-shifting Diffraction Interferometer, in Adaptive Optics Systems and Technology, SPIE Conference Series, 3762, 237

Ellerbroek, B. L., Baudoz, P., Mas, M., et al. 2010, Focal Plane Wavefront Sensor Sensitivity for ELT Planet Finder, in SPIE Conference Series, 7736, 77365S

Gonsalves, R. A. 1982, Optical Engineering, 21, 829

Hartung, M., Blanc, A., Fusco, T., et al. 2003, A&A, 399, 385

Hartung, M., Blanc, A., Fusco, T., Lacombe, F., et al. 2003, A&A, 399, 385

Hinkley, S., Oppenheimer, B. R., Zimmerman, N., et al. 2011, PASP, 123, 74

Ren, D., & Dong, B. 2012, Optical Engineering, 51, 101705

Ren, D., Dong, B., Zhu, Y., & Christian, D. J. 2012, Publications of the Astronomical Society of the Pacific, 124, 247

Ren, D., Penn, M., Wang, H., Chapman, G., & Plymate, C. 2010, in Spie Astronomical Telescopes + Instrumentation

Sauvage, J.-F., Fusco, T., Rousset, G., et al. 2005, in Astronomical Adaptive Optics Systems and Applications II, 5903, International Society for Optics and Photonics, 59030B

Sauvage, J.-F., Fusco, T., Rousset, G., & Petit, C. 2007, Journal of the Optical Society of America A, 24, 2334

Vorontsov, M. A., & Sivokon, V. P. 1998, Journal of the Optical Society of America A, 15, 2745

Vorontsov, M. A., & Yu, M. 2004, Journal of the Optical Society of America A, 21, 1659

Vorontsov, M., Carhart, G., & Ricklin, J. 1997, Optics letters, 22, 907

Wallace, J. K., Burruss, R. S., Bartos, R. D., et al. 2010, The Gemini Planet Imager Calibration Wavefront Sensor Instrument, in Adaptive Optics Systems II, SPIE Conference Series, 7736, 77365D

Wallace, J. K., Rao, S., Jensen-Clem, R. M., & Serabyn, G. 2011, Phase-shifting Zernike Interferometer Wavefront Sensor, in Optical Manufacturing and Testing IX, SPIE Conference Series, 8126, 81260F

Wang, Z., Wang, J., Wang, B., & Wu, Y. H. 2017, Optik, 129, 217